Journal of Physics: Condensed Matter

Structure of amorphous materials in the NASICON system $Na_{1+x}Ti_2Si_xP_{3-x}O_{12}$

OPEN ACCESS
IOP Publishing
Journal of Physics: Condensed Matter
J. Phys.: Condens. Matter **35** (2023) 274002 (9pp)
https://doi.org/10.1088/1361-648X/acc8af

Structure of amorphous materials in the NASICON system $Na_{1+x}Ti_2Si_xP_{3-x}O_{12}$

Rita Mendes Da Silva[1], Anita Zeidler[1], Henrik Bradtmüller[2], Hellmut Eckert[3], Henry E Fischer[4], Chris J Benmore[5] and Philip S Salmon[1,*]

[1] Department of Physics, University of Bath, Bath BA2 7AY, United Kingdom
[2] Department of Materials Engineering, Vitreous Materials Laboratory, Universidade Federal de São Carlos, Rod. Washington Luis, km 235, CP 676, São Carlos 13565-905, SP, Brazil
[3] Instituto de Física de São Carlos, Universidade de São Paulo, CP 369, São Carlos 13566-590, SP, Brazil
[4] Institut Laue Langevin, 71 Avenue des Martyrs, 38042 Grenoble Cedex 9, France
[5] X-ray Science Division, Advanced Photon Source, Argonne National Laboratory, 9700 South Cass Avenue, Lemont, Lemont, IL 60439, United States of America

E-mail: p.s.salmon@bath.ac.uk

Received 15 December 2022, revised 27 February 2023
Accepted for publication 29 March 2023
Published 13 April 2023

Abstract

The structure of glasses in the sodium (Na) super-ionic conductor (NASICON) system $Na_{1+x}Ti_2Si_xP_{3-x}O_{12}$ with $x = 0.8$ and $x = 1.0$ was explored by combining neutron and high-energy x-ray diffraction with ^{29}Si, ^{31}P and ^{23}Na solid-state nuclear magnetic resonance (NMR) spectroscopy. The ^{29}Si magic angle spinning (MAS) NMR spectra reveal that the silica component remains fully polymerized in the form of Si^4 units, i.e. the silicon atoms are bound to four bridging oxygen atoms. The $^{31}P\{^{23}Na\}$ rotational echo adiabatic passage double resonance (REAPDOR) NMR data suggest that the ^{31}P MAS NMR line shape originates from four-coordinated P^n units, where $n = 1$, 2 or 3 is the number of bridging oxygen atoms per phosphorus atom. These sites differ in their ^{31}P-^{23}Na dipolar coupling strengths. The results support an intermediate range order scenario of a phosphosilicate mixed network-former glass in which the phosphate groups selectively attract the Na^+ modifier ions. Titanium takes a sub-octahedral coordination environment with a mean Ti–O coordination number of 5.17(4) for $x = 0.8$ and 4.86(4) for $x = 1.0$. A mismatch between the P–O and Si–O bond lengths of 8% is likely to inhibit the incorporation of silicon into the phosphorus sites of the NASICON crystal structure.

Keywords: structure, NASICON, amorphous materials, solid-state NMR, neutron and x-ray diffraction

(Some figures may appear in colour only in the online journal)

* Author to whom any correspondence should be addressed.

1. Introduction

There is a quest to find Na-based solid electrolytes and electrode materials to replace those based on lithium for electrical energy storage devices, largely motivated by the low cost of Na and its widespread abundance [1–4]. Here, Na super-ionic conductor (NASICON) materials have received significant attention in view of their large Na^+ ion conductivity and structural stability in the solid state [5–7]. An example is provided by $NaTi_2(PO_4)_3$ [8, 9], where the crystal structure is based on a negatively-charged open framework that is constructed from corner-sharing octahedral TiO_6 and tetrahedral PO_4 units: each octahedron is connected to six tetrahedral units and each tetrahedron is connected to four octahedral units [10, 11]. The Na^+ ions reside in the interstitial sites of the framework, and are free to migrate between those sites.

In a crystalline material such as $NaTi_2(PO_4)_3$, a proposed strategy for increasing the ionic conductivity is to increase the Na^+ content of the material by replacing P^{5+} by Si^{4+} ions [12–14]. In this substitution, additional Na^+ ions are required to ensure charge neutrality. Such $Na_{1+x}Ti_2Si_xP_{3-x}O_{12}$ (NTSP) materials, where the composition can be re-written as $(Na_2O)_{1+x}(TiO_2)_4(SiO_2)_{2x}(P_2O_5)_{3-x}$, can be made via a glass-ceramic route, which offers an ability to control features of the microstructure, such as the porosity, via the thermal-treatment protocol chosen for the glass. This synthesis route can be used to eliminate the interfacial problems and transport impediments associated with powdered materials, and it also offers the important advantage of moldable bulk materials [15]. In recent work on the NTSP system, x-ray diffraction showed the formation of a NASICON phase for glass-ceramic compositions with $x \leqslant 0.8$ [9]. However, the lowest activation energy and largest ionic conductivity were achieved for $x = 1.0$, which lies in a range of compositions $0.8 < x \leqslant 1.2$ where the major crystalline component was found to be the non-NASICON $Na(TiO)(PO_4)$ phase. The extent to which P^{5+} ions are replaced by Si^{4+} ions within the NASICON structure remains unclear [9, 16, 17].

The glass-ceramic preparation route leads to fundamental questions regarding the structure of the parent glass and how it evolves as the system crystallizes. For instance, vitreous NASICONs typically contain fivefold and/or sixfold coordinated network-forming units [18] and thus transcend Zachariasen's rules for glass formation [19]. In consequence, they are not optimal glass-forming systems and require vitrification of the melt via a rapid-cooling technique such as splat-quenching. This complication poses basic questions about the nature of the glass topology and how this organization facilitates crystallization. For instance, in the NASICON system $Na_{1+x}Al_xGe_{2-x}(PO_4)_3$ (NAGP) with $x = 0.0$–0.8, the crystals are nucleated homogeneously, which allows for the creation, via the thermal treatment protocol, of a uniform distribution of crystallites of controllable shape and size throughout the bulk material. Here, it has been discovered that the seeds for homogeneous crystal nucleation are located on superstructural units that are built into the glass structure [18].

We have therefore been motivated to make the first structural characterization of NTSP glasses that can be used as precursors in the preparation of super-ionic glass-ceramic materials. Specifically, we investigated the structure of the NTSP glasses with $x = 0.8$ and $x = 1.0$, which lead to glass-ceramics in which either a NASICON or non-NASICON phase is the majority crystalline component, respectively. A multi-probe approach was adopted in which neutron diffraction and high-energy x-ray diffraction were combined with ^{29}Si, ^{31}P and ^{23}Na solid-state nuclear magnetic resonance (NMR) spectroscopy. A marriage of the diffraction techniques offers an effective means of identifying the mean coordination environment of titanium by exploiting (i) a negative weighting of the Ti–O correlations in neutron diffraction, which originates from the negative coherent neutron scattering length of Ti [20], versus (ii) a large positive weighting of those correlations in x-ray diffraction, which originates from the comparatively large atomic number of Ti ($Z = 22$). The solid-state NMR experiments deliver site-specific information on the Si, P and Na coordination environments.

We find that silicon and phosphorus are both four-coordinated but make a different number of connections to the glass network via bridging-oxygen (BO) atoms: The P^{5+} ions form species with either 1, 2, or 3 BO atoms whereas all the Si^{4+} ions form species with 4 BO atoms. A mismatch of 8% is also found between the P–O and Si–O bond lengths. This inequivalence is likely to inhibit the incorporation of silicon into the phosphorus sites of the NASICON crystal structure when the glass is thermally annealed, helping to promote the formation of the non-NASICON $Na(TiO)(PO_4)$ phase at larger x values. We also uncover the intermediate range order: The phosphate groups scavenge the Na^+ ions by replacing BO atoms by non-bridging oxygen (NBO) atoms to balance the charge on the Na^+ ions added when P^{5+} is replaced by Si^{4+}. Our work indicates that this replacement is not optimal for manipulating the NASICON structure to enhance its ionic conductivity, thus revealing an important design rule.

This paper is organized as follows. The essential theory for diffraction is given in section 2 and the experimental methods are described in section 3. The results are presented in section 4 and are discussed in section 5 by reference to the structure of glassy NAGP which has been investigated extensively [18, 21]. Conclusions are drawn in section 6.

2. Diffraction theory

In a neutron or x-ray diffraction experiment on a glassy system, the measured total structure factor can be written as [22]

$$S(k) = 1 + \frac{1}{\langle w(k)\rangle^2}\sum_{\alpha}\sum_{\beta} c_\alpha c_\beta w_\alpha(k) w_\beta(k)\left[S_{\alpha\beta}(k) - 1\right], \tag{1}$$

where k is the magnitude of the scattering vector. The atomic fraction of chemical species α is given by c_α and the partial structure factor for chemical species α and β is given

by $S_{\alpha\beta}(k)$. The $w_\alpha(k)$ term for chemical species α depends on the nature of the measurement probe and denotes either a k-dependent x-ray atomic form factor $f_\alpha(k)$ or a k-independent coherent neutron scattering length b_α. The mean value is given by $\langle w(k)\rangle = \sum_\alpha c_\alpha w_\alpha(k)$.

The associated real-space information is described by the total pair-distribution function

$$D'(r) = \frac{2}{\pi}\int_0^\infty \mathrm{d}k\, k\,[S(k)-1]\,M(k)\sin(kr) = D(r)\otimes M(r) \quad (2)$$

where r is a real-space distance and $\otimes$ represents the one-dimensional convolution operator. The window function $M(k)$ arises from the limited k-space range over which a diffractometer can measure, and is often represented by the step function $M(k) = 1$ for $k \leqslant k_{\max}$ and $M(k) = 0$ for $k > k_{\max}$, where $k_{\max}$ is the measurement cut-off value. Its real-space representation $M(r)$ is a symmetrical function. In the case of neutron diffraction, the total pair-distribution function is given by

$$D(r) = \frac{4\pi\rho r}{\langle b\rangle^2}\sum_\alpha\sum_\beta c_\alpha c_\beta b_\alpha b_\beta\,[g_{\alpha\beta}(r)-1], \quad (3)$$

where ρ is the atomic number density, $g_{\alpha\beta}(r)$ is a partial pair-distribution function, and the mean scattering length $\langle b\rangle = \sum_\alpha c_\alpha b_\alpha$.

To discriminate features in $D'(r)$ that originate from the glass structure from those that originate from $M(r)$, each peak or trough i in $rg_{\alpha\beta}(r)$ was described by the Gaussian function [18]

$$p^i_{\alpha\beta}(r) = \frac{1}{4\pi\rho}\frac{\bar{n}^\beta_\alpha(i)}{c^i_\beta r^i_{\alpha\beta}}\frac{1}{\sqrt{2\pi}\sigma^i_{\alpha\beta}}\exp\left[-\frac{(r-r^i_{\alpha\beta})^2}{2(\sigma^i_{\alpha\beta})^2}\right], \quad (4)$$

where $r^i_{\alpha\beta}$ is the peak position, $\sigma^i_{\alpha\beta}$ is the standard deviation, and $\bar{n}^\beta_\alpha(i)$ is the coordination number of chemical species β around α. Each peak or trough makes a contribution towards $[S(k)-1]$ given by

$$p^i_{\alpha\beta}(k) = W^i_{\alpha\beta}(k)\frac{\bar{n}^\beta_\alpha(i)}{c^i_\beta}\frac{\sin(kr^i_{\alpha\beta})}{kr^i_{\alpha\beta}}\exp\left[-\frac{k^2(\sigma^i_{\alpha\beta})^2}{2}\right], \quad (5)$$

where the weighting factor $W^i_{\alpha\beta}(k) = (2-\delta_{\alpha\beta})\,c^i_\alpha c^i_\beta\, w^i_\alpha(k)\, w^i_\beta(k)/\langle w(k)\rangle^2$ and $\delta_{\alpha\beta}$ represents the Kronecker delta. The neutron and x-ray diffraction data sets were fitted using the procedures described in [18] and the goodness-of-fit was quantified by the parameter R_χ [23].

3. Experiment

3.1. Sample preparation

The NTSP glasses were made by splat-quenching in air (oxygen partial pressure $p_{O_2} = 0.21$ bar) following the procedure described in [9]. In summary, stoichiometric quantities of powdered Na carbonate, titanium dioxide, dihydrogen ammonium phosphate and silicon dioxide were mixed for 12 h using a rotary ball mill with alumina balls. The mixture was then decomposed in a platinum crucible at a temperature between 400 °C and 700 °C for 6 h, before melting at a temperature of 1400 °C–1500 °C and equilibrating for 30 min. Finally, the melt was splat-quenched between two metal plates and the resultant glass was annealed for 2 h at a temperature 40 °C below the glass transition temperature T_g of 677(2) °C ($x = 0.8$) or 635(2) °C ($x = 1.0$). The batched compositions correspond to $x = 0.803$ and $x = 1.000$ and the oxygen content of each material follows from the glass stoichiometry. The glassy materials were grey and optically opaque and were investigated in their as-prepared state. Mass densities of 2.8719(9) g cm^{-3} ($x = 0.8$) and 2.8397(4) g cm^{-3} ($x = 1.0$) at 22.4 °C were measured using He pychnometry, corresponding to number densities of $\rho = 0.07\,747(1)$ Å^{-3} and $\rho = 0.07\,668(1)$ Å^{-3}, respectively.

3.2. Solid-state NMR

Solid-state NMR experiments were carried out on an Agilent DD2 spectrometer operating with a 5.64 T magnet and a Bruker Avance Neo spectrometer operating with a 14.1 T magnet. The ^{29}Si magic angle spinning (MAS) NMR experiments were performed at 48.15 MHz using a commercial 7.5 mm double resonance probe. A MAS frequency of 5.0 kHz was used and 1200 to 1400 transients were recorded using a 90° excitation pulse of 7.5 μs and a recycle delay of 60 s. The relatively short relaxation delay could be chosen because the samples contained paramagnetic Ti^{3+} ions at the doping level, which facilitated nuclear spin relaxation. The ^{23}Na and ^{31}P MAS NMR experiments were performed at 158.80 and 243.03 MHz, respectively, using a commercial 2.5 mm triple resonance probe operating at a MAS frequency of 15.0 kHz. For ^{23}Na, 4096 scans were collected using an excitation pulse of 0.8 μs, corresponding to a small tip-angle of 35° and a recycle delay of 1 s. For ^{31}P, 4 scans were recorded using a 90° pulse of 3 μs duration and a recycle delay of 1200 s. Chemical shifts are reported relative to tetramethylsilane (TMS), 0.1 M NaCl solution, and 85% H_3PO_4, using solid NaCl [$\delta_{iso}(^{23}Na) = 7.2$ ppm] and BPO_4 [$\delta_{iso}(^{31}P) = -29.27$ ppm] as secondary references.

The ^{31}P{^{23}Na} rotational echo adiabatic passage double resonance (REAPDOR) NMR experiments [24, 25] were performed under the same conditions as the MAS NMR experiments using a rotor-synchronized Hahn spin echo sequence (π-pulse length of 6 μs) for ^{31}P detection and a ^{23}Na adiabatic pulse of one third of a rotor period ($\nu_{nut} = 70$ kHz) for dipolar re-coupling. The π pulses applied at the observation channel were phase cycled according to the XY-8 scheme.

The ^{23}Na MAS NMR spectra were simulated assuming second-order quadrupolar line shapes and distributions of nuclear electric quadrupolar coupling constants (C_Q) according to the Czjzek model [26], implemented in the ssNake v1.5b solid state NMR spectral data processing software [27].

3.3. Neutron diffraction

The neutron diffraction experiment employed the instrument D4c at the Institut Laue-Langevin with an incident wavelength of 0.4955(1) Å [28]. Coarsely-ground glass samples were held in a cylindrical vanadium container of inner diameter 6.8 mm and wall thickness 0.1 mm. Diffraction patterns were measured at room temperature (∼298 K) for each sample in its container, the empty container, the empty instrument, a cylindrical vanadium rod of diameter 6.08(1) mm for normalization purposes, and a neutron absorbing $^{10}B_4C$ bar of size comparable to the sample in order to estimate the effect at small scattering angles of the sample self-shielding on the background count-rate [29]. The data sets were corrected using a standard procedure [30]. Neutron scattering lengths of $b_{Na} = 3.63(2)$ fm, $b_{Ti} = -3.438(2)$ fm, $b_{Si} = 4.1491(10)$ fm, $b_P = 5.13(1)$ fm and $b_O = 5.803(4)$ fm [20] were used in the data analysis.

3.4. X-ray diffraction

The x-ray diffraction experiment employed beamline 6-ID-D at the Advanced Photon Source with an incident x-ray energy of 100.233 keV. Powdered glass samples were held in cylindrical Kapton polyimide tubes of 1.80(1) mm internal diameter and 0.051(6) mm wall thickness. The scattered x-rays were counted using a Varex 4343CT amorphous silicon flat panel detector placed at a distance of 311 mm from the sample position, as found from the diffraction pattern measured for crystalline CeO_2. Diffraction patterns were measured at room temperature for each sample in its container, an empty container and the empty instrument. The two-dimensional images were converted to one-dimensional diffraction patterns using FIT2D [31]. The data sets were corrected for background scattering, beam polarization, attenuation, and Compton scattering using PDFgetX2 [32]. Neutral atom form-factors were used in the data analysis [33].

4. Results

4.1. NMR results

Figure 1 shows the measured ^{29}Si, ^{23}Na, and ^{31}P single-pulse MAS NMR spectra for both of the NTSP samples, together with the fitted curves.

Each ^{29}Si NMR spectrum can be fitted, within the attained signal-to-noise ratio, to a single Gaussian peak centered at an isotropic chemical shift typical of fully polymerized silicon (Si^4) species (table 1), which do not bear NBO atoms. This result indicates that, within the glassy NTSP mixed network-former system, the network-former P_2O_5 acts as an alkali network-modifier scavenger, i.e. the phosphorus atoms bind to the NBO atoms and therefore compete very effectively against silicon in attracting the alkali ions. Similar behavior has been noted for Na phosphosilicate glasses with similar compositions [34, 35].

The ^{23}Na MAS NMR spectra are typical of those observed for glassy materials. Each spectrum shows an asymmetric line shape, which reflects the second-order quadrupolar perturbation effects on the Zeeman frequencies in the presence of a distribution of electric field gradients. The isotropic chemical shift values, δ_{iso}, (table 1) are typical of those observed in Na phosphate glasses with comparable Na/P ratios. They are similar to the values measured in glassy $Na_{1+x}Al_xTi_{2-x}(PO_4)_3$ (NATP) [21], but are more negative than the values measured in binary Na phosphate [36] and quaternary Na_2O–SiO_2–P_2O_5–Al_2O_3 glasses [35]. In all these systems, including the present NTSP glasses, the δ_{iso} values tend to increase with increasing Na/P ratio. The latter effect is attributed to an increased probability of two Na^+ ions sharing the same NBO atom and is likely associated with a decreasing Na–O coordination number and/or bond distance, which is often ascribed to increased Na–O bond covalency [36–39].

In figure 1, the ^{31}P spectra span an overall chemical shift range of about 40 ppm. While the asymmetry of the line shape,

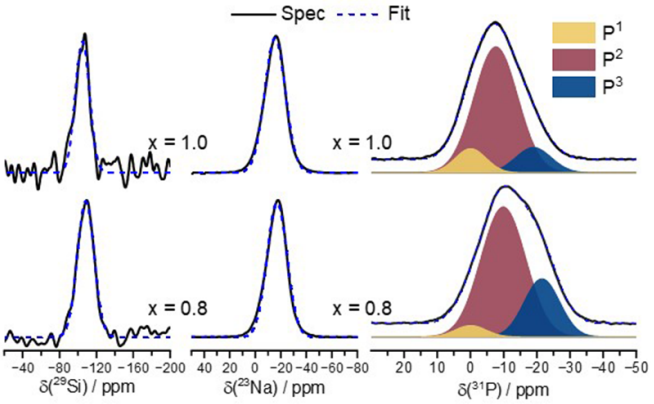

Figure 1. The ^{29}Si (left column), ^{23}Na (central column), and ^{31}P (right column) MAS NMR spectra for the NTSP glasses with $x = 0.8$ (bottom row) and $x = 1.0$ (top row). The measured spectra are shown by the solid curves and the fits are shown by the broken curves. For the ^{31}P data sets, the yellow, brown, and blue components are assigned to the P^1, P^2, and P^3 species, respectively.

Table 1. Fitting parameters for the ^{29}Si, ^{23}Na, and ^{31}P single-pulse MAS NMR line shapes. The listed parameters are the mean isotropic chemical shift δ_{iso}, fractional areas for the P^n species in the ^{31}P spectra, average absolute value for the ^{23}Na quadrupolar coupling constant (center of the distribution) $\langle|C_Q|\rangle$, and full-width at half-maximum (FWHM) of a Gaussian broadened (GB) distribution of isotropic chemical shifts.

x	Resonance	δ_{iso} (±2 ppm)	Area (±2%)	$\langle\|C_Q\|\rangle$ (±0.05 MHz)	FWHM GB (±1 ppm)
0.8	^{29}Si	−108.3	—	—	21.3
	^{23}Na	−15.9	—	0.90	18.4
	^{31}P–P^1	−0.1	4	—	11.0
	^{31}P–P^2	−9.9	71	—	15.9
	^{31}P–P^3	−21.6	25	—	13.0
1.0	^{29}Si	−104.3	—	–	16.0
	^{23}Na	−13.4	—	1.28	18.4
	^{31}P–P^1	−0.1	10	—	12.7
	^{31}P–P^2	−7.7	77	—	15.5
	^{31}P–P^3	−19.0	13	—	11.0

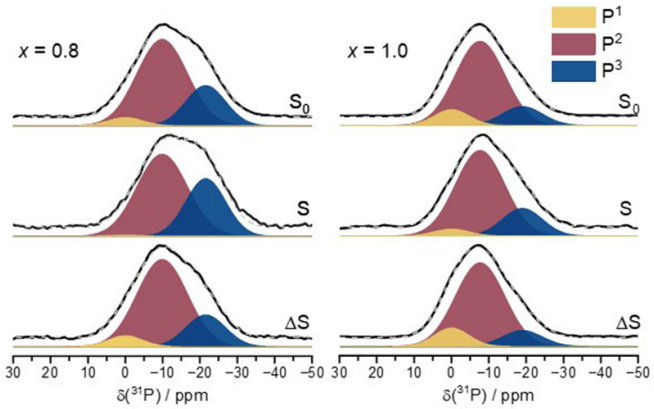

Figure 2. The S_0 (top row), S (middle row) and ΔS (bottom row) NMR spectra from ^{31}P{^{23}Na} REAPDOR NMR experiments for the NTSP glasses with $x = 0.8$ (left column) and $x = 1.0$ (right column). The dipolar mixing time was 1.6 ms. The measured spectra are shown by the solid curves and the fits are shown by the broken curves. The yellow, brown, and blue components are assigned to the P^1, P^2, and P^3 species, respectively.

Table 2. Average isotropic chemical shift δ_{iso}, FWHM, and fractional areas obtained from the single-pulse ^{31}P MAS NMR spectra, rotor-synchronized spin echo spectra S_0, dipolar re-coupled spectra S after a mixing time of 1.6 ms, and the corresponding difference signals $\Delta S = S_0 - S$.

		δ_{iso} (±5 ppm)			FWHM GB (±1 ppm)			Fractional area (±2%)		
x	Signal	P^1	P^2	P^3	P^1	P^2	P^3	P^1	P^2	P^3
0.8	MAS NMR	−0.1	−9.9	−21.6	11.0	15.9	13.0	4	71	25
	S_0	−0.1	−9.9	−21.6	11.0	15.9	13.0	5	70	26
	S	−0.1	−9.9	−21.6	11.0	15.9	13.0	1	64	35
	ΔS	−0.1	−9.9	−21.6	11.0	15.9	13.0	6	73	21
1.0	MAS NMR	−0.1	−7.7	−19.0	12.7	15.5	11.0	10	77	13
	S_0	−0.1	−7.7	−19.0	12.7	15.5	11.0	10	76	14
	S	−0.1	−7.7	−19.0	12.7	15.5	11.0	4	76	20
	ΔS	−0.1	−7.7	−19.0	12.7	15.5	11.0	12	76	12

which is particularly marked for the $x = 0.8$ composition, suggests a superposition of several components, the poor resolution makes it impossible to arrive at a unique fitting model. One promising approach for developing some deconvolution constraints is the use of ^{31}P{^{23}Na} REAPDOR experiments, which may distinguish between the phosphate units with different ^{31}P-^{23}Na dipolar coupling strengths [18, 35]. The spectra shown in the top row of figure 2 are the rotor synchronized MAS spin-echo signals S_0 after 24 rotor periods (1.6 ms after the 90° preparation pulse.) The line shapes are essentially identical to those found for the single-pulse spectra in figure 1. The middle and bottom rows of figure 2 show the spectra obtained with dipolar re-coupling, S, and the difference signal $\Delta S = S_0 - S$. Note that the lineshapes of S and ΔS differ significantly. For both materials, the difference signal is more pronounced on the higher (less negative) frequency side than on the lower (more negative) frequency side of the MAS NMR line shape, indicating distinct differences in the ^{31}P-^{23}Na dipolar coupling strengths. A consistent deconvolution of each spectrum into three components near 0, −9, and −20 ppm can be obtained for both NTSP materials (table 2), from which the average phosphate connectivity $\langle n \rangle = [P^1] + 2[P^2] + 3[P^3]$ can be determined from the fitted areas, where $[P^n]$ represents the fraction of species P^n and n denotes the number of bridging oxygen atoms per phosphorus atom (see the appendix). From the ^{31}P MAS NMR spectra, we find $\langle n \rangle$ = 2.21(3) and 2.03(3) for the x = 0.8 and 1.0 compositions, respectively.

The results are very close to those predicted for a network modification scenario in which the phosphate species selectively attract the alkaline network modifier, leaving the silica and titania components unmodified. In this scenario, the charge on the Na^+ ions is balanced by the charge on the phosphate groups such that the mean number of BO atoms per phosphorus atom is given by $\langle n \rangle = 3 - (1 + x)/(3 - x)$ (see the appendix). The modeled values depend on the Na/P ratio and are $\langle n \rangle = 2.18$ for $x = 0.8$ versus $\langle n \rangle = 2.00$ for $x = 1.0$. This decrease in $\langle n \rangle$ with increasing x arises from the need of the phosphate groups to incorporate an increased number of NBO atoms to balance the charge on the increased number of Na^+ ions. The ^{31}P MAS NMR results show this is achieved via an increase in the fraction of negatively charged P^1 units and a decrease in the fraction of charge neutral P^3 units (table 2). We may thus conclude that the solid-state NMR data are consistent with this network modification scenario, which is further supported by the ^{29}Si MAS NMR experiments and the ^{23}Na

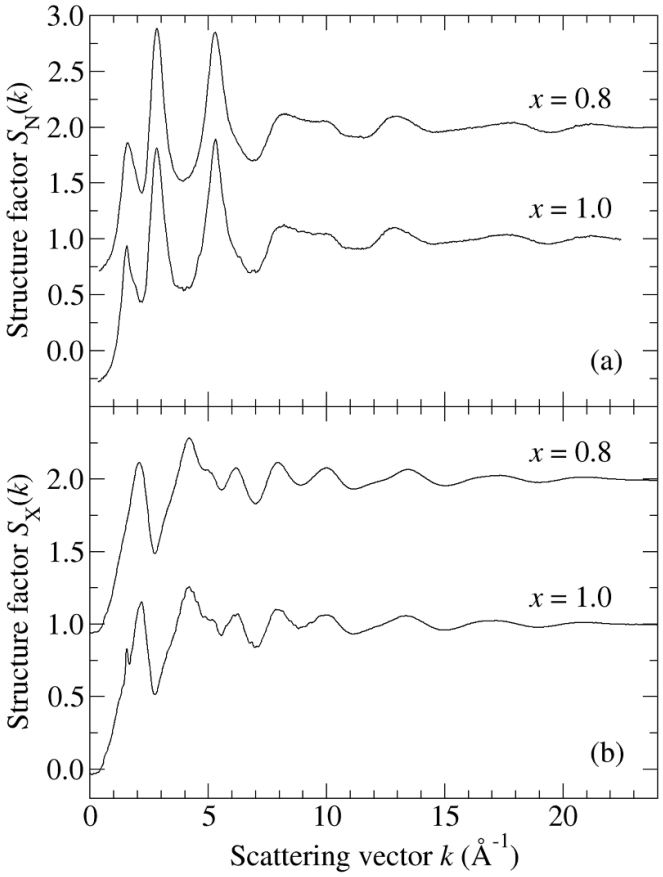

Figure 3. The measured (a) neutron and (b) x-ray total structure factors for the NTSP glasses with $x = 0.8$ and $x = 1.0$. The $x = 0.8$ data sets are shifted upwards for clarity of presentation.

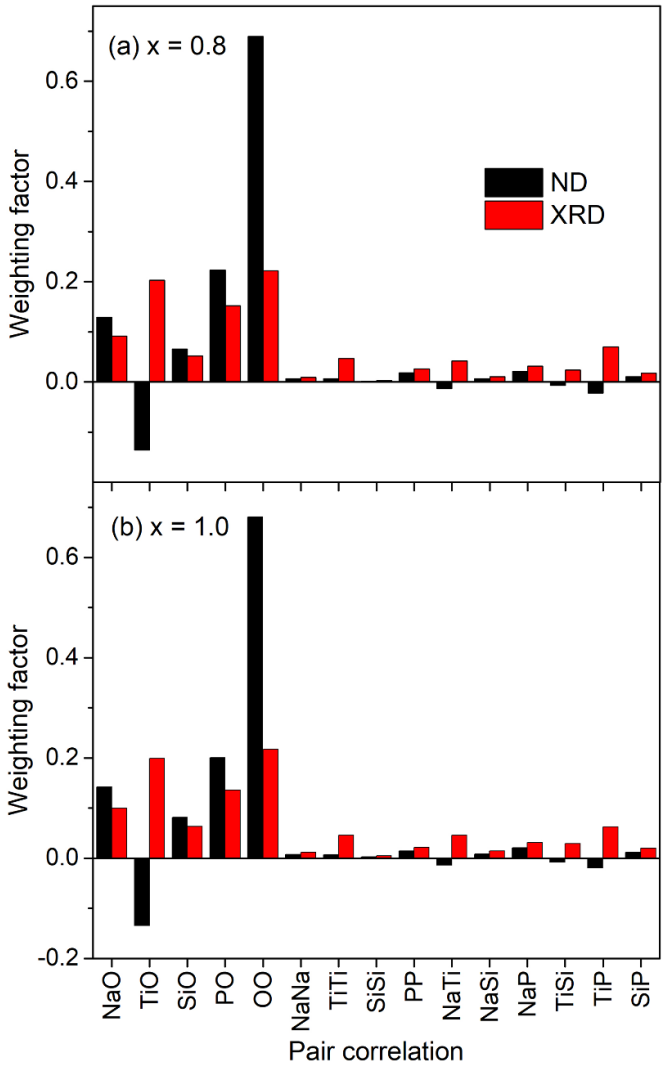

Figure 4. The weighting factors $W_{\alpha\beta}(k) = (2 - \delta_{\alpha\beta})\, c_\alpha c_\beta w_\alpha(k)\, w_\beta(k) / \langle w(k) \rangle^2$ given to the partial structure factors for the neutron diffraction (ND) versus x-ray diffraction (XRD) experiments on the NTSP glasses with (a) $x = 0.8$ and (b) $x = 1.0$ (see equation (1)). The x-ray values were calculated for $k = 0$.

isotropic chemical shift data. The ^{23}Na shifts in Na silicate glasses, where Na interacts with the NBO atoms linked to silicon, are found at significantly higher values than those measured here [40].

4.2. Diffraction results

For a given composition, the measured $S(k)$ functions of figure 3 show substantial differences between the neutron and x-ray diffraction patterns, in accordance with the different weighting factors for the partial structure factors (figure 4). The x-ray diffraction results for $x = 1.0$ show a small Bragg peak at $\simeq$1.55 Å^{-1}. A reliable identification of the associated phase is not possible on the basis of a single peak. The amount of this phase in the bulk-prepared material is, however, small as judged by the small size of the Bragg peak, the absence of Bragg peaks in the neutron diffraction data, and the absence of sharp features in any of the MAS NMR spectra.

The $D'(r)$ functions measured by neutron and x-ray diffraction are shown in figures 5 and 6, respectively. In the fitting procedure, the first peak in $D'(r)$ at $\simeq$1.54 Å was attributed to P-O and Si-O correlations and the second feature in $D'(r)$ at $\simeq$1.95 Å was attributed to Ti-O correlations. The latter appears as a trough in the neutron diffraction work, on account of the negative scattering length of Ti, but as a peak in the x-ray diffraction work, on account of the large atomic number of Ti (figure 4). In comparison with the structure of crystalline $NaTi_2(PO_4)_3$, the nearest-neighbor Na–O correlations are expected to appear in $D'(r)$ at around 2.29–2.50 Å [10, 11]. For tetrahedral PO_4 and SiO_4 motifs with P–O and Si–O bond distances of $r_{PO} = 1.526$ Å and $r_{SiO} = 1.647$ Å, respectively, the nearest-neighbor O–O correlations are expected to contribute towards $D'(r)$ at about $r_{OO} = \sqrt{8/3} r_{PO} = 2.492$ Å and $r_{OO} = \sqrt{8/3} r_{SiO} = 2.690$ Å, respectively. The Na–O and O–O correlations in the $D'(r)$ functions were introduced into the fitting procedure in order to constrain the peaks fitted at smaller r-values, but the associated peak parameters

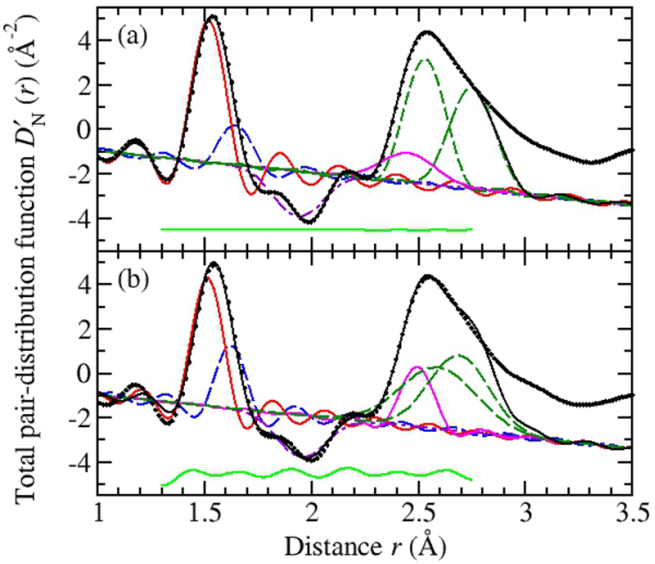

Figure 5. The fitted neutron functions $D'_N(r)$ for the NTSP glasses with (a) $x = 0.8$ and (b) $x = 1.0$. In each panel, the solid circles represent the measured function, the black solid curve shows the fitted function, and the other curves give the contributions from the P–O (red solid curve), Si–O (blue broken curve), Ti–O (violet chained curve), Na–O (magenta solid curve) and O–O (green broken curves) correlations. The residual is given by the displaced green solid curve. The Na–O and O–O correlations were used to place constraints on the peaks fitted at smaller r-values.

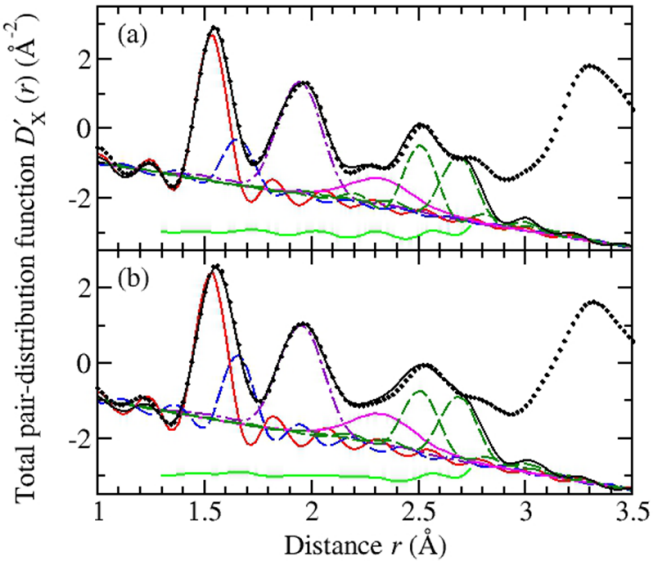

Figure 6. The fitted x-ray functions $D'_X(r)$ for the NTSP glasses with (a) $x = 0.8$ and (b) $x = 1.0$. In each panel, the solid circles represent the measured function, the black solid curve shows the fitted function, and the other curves give the contributions from the P–O (red solid curve), Si–O (blue broken curve), Ti–O (violet chained curve), Na–O (magenta solid curve) and O–O (green broken curves) correlations. The residual is given by the displaced green solid curve. The Na–O and O–O correlations were used to place constraints on the peaks fitted at smaller r-values.

are uncertain because of peak overlap. The fitted P–O, Si–O and Ti–O peak parameters obtained from the neutron and x-ray $D'(r)$ functions are summarized in tables 3 and 4, respectively.

Table 3. Parameters obtained from Gaussian peak fits to the r-space functions for the NTSP glasses with $x = 0.8$ and $x = 1.0$ measured using neutron diffraction. The fitted functions are shown in figure 5. R_χ is given for the fitted range 1.30–2.75 Å.

x	Atom pair	$r_{\alpha\beta}$ (Å)	$\sigma_{\alpha\beta}$ (Å)	$\bar{n}^\beta_\alpha$	R_χ (%)
0.8	P–O	1.522(2)	0.026(5)	4.01(2)	0.84
	Si–O	1.648(3)	0.020(4)	4.01(2)	
	Ti–O	1.939(4)	0.110(6)	5.16(4)	
1.0	P–O	1.517(2)	0.041(4)	4.00(2)	5.35
	Si–O	1.623(3)	0.005(5)	4.00(2)	
	Ti–O	1.955(4)	0.111(6)	4.85(4)	

Table 4. Parameters obtained from Gaussian peak fits to the r-space functions for the NTSP glasses with $x = 0.8$ and $x = 1.0$ measured using x-ray diffraction. The fitted functions are shown in figure 6. R_χ is given for the fitted range 1.30–2.74 Å.

x	Atom pair	$r_{\alpha\beta}$ (Å)	$\sigma_{\alpha\beta}$ (Å)	$\bar{n}^\beta_\alpha$	R_χ (%)
0.8	P–O	1.535(1)	0.038(1)	4.00(1)	5.98
	Si–O	1.659(1)	0.038(3)	4.00(1)	
	Ti–O	1.949(1)	0.108(1)	5.17(4)	
1.0	P–O	1.531(1)	0.032(1)	4.00(1)	5.81
	Si–O	1.658(1)	0.010(5)	4.00(1)	
	Ti–O	1.954(1)	0.111(1)	4.87(3)	

5. Discussion

The ^{29}Si and ^{31}P solid-state NMR and diffraction results are consistent with a glass network built from tetrahedral PO_4 and SiO_4 motifs. The connectivity of these species is, however, quite different, with the phosphorus atoms forming P^1, P^2 or P^3 units and the silicon atoms forming Si^4 units alone. P^4 units, which are the only phosphate species present in the NASICON structure of crystalline materials such as $NaTi_2(PO_4)_3$ (section 1), are notable by their absence. The mean Si–O bond length of 1.647 Å is 8% longer than the mean P–O bond length of 1.526 Å, leading to tetrahedral volumes of 2.293 and 1.825 Å^3, respectively. The volume of a SiO_4 tetrahedron is, therefore, 26% larger than that of a PO_4 tetrahedron. In comparison, for the crystal structure of $Na_5Ti_2(Si_2O_9)(PO_4)$, in which tetrahedral SiO_4 and PO_4 units coexist [41, 42], the Si-O bond length is 4%–5% longer than the mean P–O bond length, leading to a tetrahedral volume that is 12%–17% larger for SiO_4 compared to PO_4. In contrast, for the NAGP system, where the strategy for increasing the ionic conductivity is to increase the concentration of Na^+ ions by replacing Ge^{4+} ions at the octahedral sites of the NASICON crystal structure by Al^{3+} ions, the Ge–O and Al–O bond distances obtained from powder diffraction are equivalent [18]. In the alumina free precursor glass, the majority of phosphorus atoms form P^3 units but there is also a substantial proportion of P^4 units.

The difference between the phosphorus and silicon atom coordination environments found for the NTSP system is likely to inhibit the incorporation of Si^{4+} ions into the P^{5+}

sites of the NASICON $NaTi_2(PO_4)_3$ crystal structure. Indeed, in experiments on the $Na_{1+x}Ti_yZr_{2-y}Si_xP_{3-x}O_{12}$ system ($0 \leqslant x \leqslant 3$, $0 \leqslant y \leqslant 2$), which were aimed at finding the influence on the ionic conductivity of substituting Zr^{4+} by Ti^{4+} ions at fixed x, it was suggested that the framework for the fully titanium substituted NASICON with $y = 2$ does not accept the substitution of PO_4 by SiO_4 groups [43]. More recent work on NTSP materials prepared via the glass-ceramic route shows the formation of a NASICON phase, where the incorporation of Si into this phase was inferred from an increase in the unit cell volume with silicon content, as smaller PO_4 units are replaced by larger SiO_4 units [9]. However, as the silicon content increases, there is a sharp drop in the fraction of the NASICON phase formed at $x = 1.0$, which is accompanied by a sharp rise in the fraction of crystalline $Na(TiO)(PO_4)$, and the NASICON phase is absent for the NTSP compositions with $x > 1.4$. A progressive instability of the NASICON phase with increasing x is also found in other work [17].

In crystalline $NaTi_2(PO_4)_3$, the Ti atoms are in an octahedral coordination environment with three shorter Ti–O bonds of length 1.884–1.896 Å and three longer Ti–O bonds of length 1.964–2.107 Å [10, 11]. By comparison, in glassy NTSP the mean Ti–O coordination number is 5.17(4) for $x = 0.8$ and 4.86(4) for $x = 1.0$. The Ti coordination environment is, therefore, sub-octahedral, as found for the coordination environment of its Ge and Al counterparts in glassy NAGP [18]. The Ti–O bond length is anticipated to increase with the Ti–O coordination number to allow the Ti-centered polyhedra to incorporate a larger number of oxygen nearest-neighbors. The mean Ti–O bond length is, however, 1.944(5) Å for $x = 0.8$ and 1.955(4) Å for $x = 1.0$. This observation does not appear to be related to distortion of the Ti-centered polyhedra because the fitted peak width for the Ti–O nearest-neighbors is comparable for both of the investigated glass compositions (tables 3 and 4).

6. Conclusions

The structure of glasses in the NASICON system $Na_{1+x}Ti_2Si_xP_{3-x}O_{12}$ (NTSP) with $x = 0.8$ and $x = 1.0$ was investigated by combining diffraction with solid-state NMR spectroscopy. The results show network structures built from tetrahedral PO_4 and SiO_4 units in which the titanium atoms reside within a sub-octahedral coordination environment. The solid-state ^{31}P NMR spectra are consistent with a structural scenario in which the phosphate groups selectively attract the Na^+ ions, producing P^1, P^2, and P^3 units whose proportions are determined by the Na/P ratio. In this process the silica component remains largely unmodified, as indicated by the Si^4 speciation found from the ^{29}Si MAS NMR experiments, and there is a small change associated with the titania component, as found from the diffraction experiments: The Ti–O coordination number decreases from $\bar{n}^{O}_{Ti} = 5.17(4)$ at $x = 0.8$ to $\bar{n}^{O}_{Ti} = 4.86(4)$ at $x = 1.0$ as P_2O_5 is replaced by SiO_2. The mismatch found between the phosphorus and silicon coordination environments, which includes a difference of 8% between the P–O and Si–O bond lengths, is likely to inhibit the incorporation of Si^{4+} ions into the P^{5+} sites of the NASICON crystal structure as the glass is annealed, thus uncovering an important design rule.

Data availability statement

The data that support the findings of this study are openly available at the following URL/DOI: https://doi.org/10.15125/BATH-01226 [44]. The measured neutron diffraction data sets are available from [45].

Acknowledgment

We are grateful to Adriana M Nieto-Muñoz and Ana Candida M. Rodrigues (Universidade Federal de São Carlos) for providing the glassy samples. R M D S acknowledges funding and support from the Royal Society (Grant No. RGF/EA/180060). A Z was supported by a Royal Society-EPSRC Dorothy Hodgkin Research Fellowship. Support by FAPESP, Project 2013/07793-6, is gratefully acknowledged. H B also thanks FAPESP for support for a post-doctoral fellowship, process 2019/26399-3. We acknowledge use of the Engineering and Physical Sciences Research Council (EPSRC) funded National Chemical Database Service hosted by the Royal Society of Chemistry. This research used resources of the Advanced Photon Source, a U.S. Department of Energy (DOE) Office of Science User Facility operated for the DOE Office of Science by Argonne National Laboratory under Contract No. DE-AC02-06CH11357.

Appendix. Phosphate connectivity

Consider NTSP glasses of composition given by the formula unit $Na_{1+x}Ti_2Si_xP_{3-x}O_{12}$. The ^{31}P MAS NMR experiments show that all the phosphorus atoms are four-coordinated in P^n phosphate groups, where $n = 1$, 2 or 3 is the number of BO atoms per phosphorus atom. Each P^n group carries a formal charge $q_{P^n} = n - 3$ in units of the elementary charge, i.e. $q_{P^1} = -2$, $q_{P^2} = -1$ and $q_{P^3} = 0$. If $[P^n]$ is the fraction of P^n groups in the glass, then the mean number of BO atoms per phosphate group is given by $\langle n \rangle = [P^1] + 2[P^2] + 3[P^3]$ where $[P^1] + [P^2] + [P^3] = 1$. The mean charge per phosphate group follows from

$$q_{P^{\langle n \rangle}} = \langle n \rangle - 3. \tag{A.1}$$

The ^{29}Si MAS NMR experiments show that all the silicon atoms are connected to 4 BO atoms, i.e. they form charge neutral Si^4 species that cannot contribute to balancing the charge on the Na^+ ions. Negatively charged phosphate groups must therefore scavenge the available Na^+ ions, and local charge neutrality requires

$$N_{Na}q_{Na} + N_P q_{P^{\langle n \rangle}} = 0, \tag{A.2}$$

where $N_{Na} = (1 + x)$ and $N_P = (3 - x)$ are the numbers of Na and P atoms within the formula unit, respectively, and

$q_{Na} = +1$ is the charge on an Na^+ ion. It follows from equation (A.2) that

$$\langle n \rangle = 3 - N_{Na}/N_P = 3 - (1+x)/(3-x). \quad (A.3)$$

All the silicon atoms form Si^4 species, so all the NBO atoms must reside in the phosphate groups. The mean number of NBO atoms per phosphorus atom is given by $N_{NBO}/N_P = 4 - \langle n \rangle = 4/(3-x)$. In consequence, $N_{NBO} = 4$, i.e. the fraction of NBO atoms $N_{NBO}/N_O = 4/12 = 1/3$. Note that overall charge neutrality is assured, i.e.

$$N_{Na}q_{Na} + N_{Ti}q_{Ti} + N_{Si}q_{Si} + N_P q_P + N_O q_O = 0, \quad (A.4)$$

since $N_{Ti} = 2$, $N_{Si} = x$, $q_{Ti} = q_{Si} = +4$, $q_P = +5$, $N_O = 12$ and $q_O = -2$.

ORCID iDs

Rita Mendes Da Silva https://orcid.org/0000-0001-6455-3710
Anita Zeidler https://orcid.org/0000-0001-6501-8525
Henrik Bradtmüller https://orcid.org/0000-0001-7971-2163
Hellmut Eckert https://orcid.org/0000-0002-6536-0117
Henry E Fischer https://orcid.org/0000-0002-1204-0750
Chris J Benmore https://orcid.org/0000-0001-7007-7749
Philip S Salmon https://orcid.org/0000-0001-8671-1011

References

[1] Ellis B L and Nazar L F 2012 *Curr. Opin. Solid State Mater. Sci.* **16** 168
[2] Su H, Jaffer S and Yu H 2016 *Energy Storage Mater.* **5** 116
[3] Jamesh M I and Prakash A S 2018 *J. Power Sources* **378** 268
[4] Chayambuka K, Mulder G, Danilov D L and Notten P H L 2018 *Adv. Energy Mater.* **8** 1800079
[5] Anantharamulu N, Rao K K, Rambabu G, Kumar B V, Radha V and Vithal M 2011 *J. Mater. Sci.* **46** 2821
[6] Chen S, Wu C, Shen L, Zhu C, Huang Y, Xi K, Maier J and Yu Y 2017 *Adv. Mater.* **29** 1700431
[7] Singh B, Wang Z, Park S, Gautam G S, Chotard J-N, Croguennec L, Carlier D, Cheetham A K, Masquelier C and Canepa P 2021 *J. Mater. Chem.* A **9** 281
[8] Zhang H, Qin B, Buchholz D and Passerini S 2018 *ACS Appl. Energy Mater.* **1** 6425
[9] Nieto-Muñoz A M, Ortiz-Mosquera J F and Rodrigues A C M 2019 *Electrochim. Acta* **319** 922
[10] Ivanov Y A, Belokoneva E L, Egorov-Tismenko Y K, Simonov M A and Belov N V 1980 *Dokl. Akad. Nauk SSSR* **252** 1122 (available at: www.mathnet.ru/eng/dan43675)
[11] Liu J *et al* 2014 *Chem. Mater.* **26** 3295
[12] Hong H Y-P 1976 *Mater. Res. Bull.* **11** 173
[13] Goodenough J B, Hong H Y-P and Kafalas J A 1976 *Mater. Res. Bull.* **11** 203
[14] Fu J 1997 *J. Am. Ceram. Soc.* **80** 1901
[15] Fu J 1997 *Solid State Ion.* **104** 191
[16] Kishioka A, Miyazawa Y, Itatani K, Howell F S and Kinoshita M 1994 *J. Ceram. Soc. Japan* **102** 155
[17] Tsuji A, Takahashi H and Oi T 2003 *J. Mater. Chem.* **13** 542
[18] Gammond L V D *et al* 2021 *J. Chem. Phys.* **155** 074501
[19] Zachariasen W H 1932 *J. Am. Chem. Soc.* **54** 3841
[20] Sears V F 1992 *Neutron News* **3** 26
[21] Bradtmüller H, Nieto-Muñoz A M, Ortiz-Mosquera J F, Rodrigues A C M and Eckert H 2018 *J. Non-Cryst. Solids* **489** 91
[22] Fischer H E, Barnes A C and Salmon P S 2006 *Rep. Prog. Phys.* **69** 233
[23] Grimley D I, Wright A C and Sinclair R N 1990 *J. Non-Cryst. Solids* **119** 49
[24] Gullion T 1995 *Chem. Phys. Lett.* **246** 325
[25] Gullion T 1997 *Magn. Reson. Rev.* **17** 83
[26] Czjzek G, Fink J, Götz F, Schmidt H, Coey J M D, Rebouillat J-P and Liénard A 1981 *Phys. Rev.* B **23** 2513
[27] van Meerten S G J, Franssen W M J and Kentgens A P M 2019 *J. Magn. Reson.* **301** 56
[28] Fischer H E, Cuello G J, Palleau P, Feltin D, Barnes A C, Badyal Y S and Simonson J M 2002 *Appl. Phys.* A **74** S160
[29] Bertagnolli H, Chieux P and Zeidler M D 1976 *Mol. Phys.* **32** 759
[30] Salmon P S, Xin S and Fischer H E 1998 *Phys. Rev.* B **58** 6115
[31] Hammersley A P 2016 *J. Appl. Cryst.* **49** 646
[32] Qiu X, Thompson J W and Billinge S J L 2004 *J. Appl. Cryst.* **37** 678
[33] Waasmaier D and Kirfel A 1995 *Acta Cryst.* A **51** 416
[34] Dupree R, Holland D, Mortuza M G, Collins J A and Lockyer M W G 1988 *J. Non-Cryst. Solids* **106** 403
[35] Lograd M, Eckert H, Ikeda H, Nakane S and Yamazaki H 2022 *J. Non-Cryst. Solids* **579** 121366
[36] Strojek W and Eckert H 2006 *Phys. Chem. Chem. Phys.* **8** 2276
[37] Xue X and Stebbins J F 1993 *Phys. Chem. Miner.* **20** 297
[38] George A M and Stebbins J F 1995 *Am. Mineral.* **80** 878
[39] George A M, Sen S and Stebbins J F 1997 *Solid State Nucl. Magn. Reson.* **10** 9
[40] Charpentier T, Ispas S, Profeta M, Mauri F and Pickard C J 2004 *J. Phys. Chem.* B **108** 4147
[41] Rastsvetaeva R K, Simonov V I and Belov N V 1971 *Dokl. Akad. Nauk SSSR* **197** 81 (available at: www.mathnet.ru/eng/dan36035)
[42] Belov N V, Gavrilova G S, Solov'eva L P and Khalilov A D 1977 *Dokl. Akad. Nauk SSSR* **235** 1064 (available at: www.mathnet.ru/eng/dan41176)
[43] Shimazu K, Yamamoto Y, Saito Y and Nakamura O 1995 *Solid State Ion.* **79** 106
[44] Salmon P S and Zeidler A 2023 Structure of amorphous materials in the NASICON system $Na_{1+x}Ti_2Si_xP_{3-x}O_{12}$ (Bath: University of Bath Research Data Archive) (https://doi.org/10.15125/BATH-01226)
[45] Salmon P S, Eckert H, Fischer H E, Gammond L V D, Mendes Da Silva R, Mohammadi H and Zeidler A 2019 Structural change in phosphate-based glassy precursors to superionic conducting glass-ceramic electrolytes (Grenoble: Institut Laue-Langevin) (https://doi.org/10.5291/ILL-DATA.6-05-1009)